3-1-2023

Microlayer evaporation governs heat transfer enhancement during pool boiling from microstructured surfaces

M. Bongarala

Han Hu

Justin Weibel
jaweibel@purdue.edu

Suresh V. Garimella

Bongarala, M.; Hu, Han; Weibel, Justin; and Garimella, Suresh V., "Microlayer evaporation governs heat transfer enhancement during pool boiling from microstructured surfaces" (2023). *CTRC Research Publications.* Paper 396.
http://dx.doi.org/https://doi.org/10.1063/5.0090156

Microlayer Evaporation Governs Heat Transfer Enhancement during Pool Boiling from Microstructured Surfaces

Manohar Bongarala [a], Han Hu [b], Justin A. Weibel [a,1], and Suresh V. Garimella [a,c]

[a] School of Mechanical Engineering and Birck Nanotechnology Center, Purdue University, West Lafayette, IN 47907 USA

[b] Department of Mechanical Engineering, University of Arkansas, Fayetteville, AR 72701 USA

[c] University of Vermont, Burlington, VT 05405 USA

Abstract:

Enhancement of the rate of boiling heat transfer, a critically significant need across a range of industrial transport processes, can be achieved by the introduction of surface microstructures. But the precise mechanism of such enhancement is not definitively understood. We establish microlayer evaporation from the imbibed liquid layer underneath the growing vapor bubbles as the key mechanism of enhancement in boiling heat transfer coefficient for microstructured surfaces. We experimentally characterize nucleate boiling heat transfer performance on silicon surfaces custom-fabricated with controlled microstructures using HFE-7100 as the working fluid. We then undertake an analytical prediction of the microlayer evaporation from the microstructured surface. A clear dependence of the measured boiling heat transfer coefficients from microstructures of different dimensions on the predicted evaporation heat transfer coefficients allows us to conclude that microlayer evaporation governs the boiling enhancement from microstructured surfaces.

Boiling offers an effective means of energy transfer for the thermal management of electronics, steam generation in power plants and nuclear reactors, refrigeration, and boilers in

[1] Corresponding author. E-mail: jaweibel@purdue.edu (J.A. Weibel)

refineries and chemical processing plants. System performance and efficiencies in these applications are often limited by the need to dissipate higher heat fluxes at some acceptable source/surface temperature. Designing enhanced thermal management systems for such applications requires an understanding of the underlying boiling heat transfer mechanisms that affect heat dissipation performance. The efficacy of boiling can be characterized in terms of two performance characteristics: the nucleate boiling heat transfer coefficient that determines that rate of heat transfer at a given surface temperature; and the upper operational limit called the critical heat flux (CHF). Critical heat flux in boiling occurs when the vapor generated completely blankets and insulates the heated surface, thus cutting off the liquid supply and resulting in a catastrophic temperature rise[1]. Both the heat transfer coefficient and CHF must be further enhanced to keep pace with increasing demands in the cooling of high-power electronic devices, and to enable cost/efficiency improvements in various energy sector applications.. For example, in the electronics industry where passive immersion cooling by boiling has the potential for significant power consumption savings for data centers and telecom stations (approximately 58% improvement in power usage effectiveness[2]), such performance improvements can be limited by the need to use electrically insulating dielectric fluids (with poor thermal properties)[3]. And in energy generation and desalination applications, enhanced boiling heat transfer coefficients allow for a reduction in the size of evaporators/heat exchangers which leads to reduce initial costs, while an enhanced CHF allows the system to operate at higher temperatures leading to overall improvement in efficiencies[4].

While boiling can be enhanced by *active* means such as by pumping the coolant across the heated surface, *passive* enhancement methods are more attractive due to their comparative simplicity. Enhancement of boiling heat transfer performance using surface modifications has been

a long-standing area of research with the exploration of approaches like surface roughness[5–8], wettability[9,10], porous coatings[11,12], and micro/nano-structuring[13–21]. Recent efforts have leveraged silicon microfabrication techniques to produce highly ordered surfaces that allow for precise control of key surface characteristics such as the roughness, cavity size, and contact angle to study the fundamental mechanisms of boiling. Most prior efforts in understanding boiling heat transfer enhancement on structured surfaces have focused on delineating the mechanisms of CHF enhancement. Previously proposed CHF enhancement mechanisms include roughness-enhanced surface forces[15], enhanced contact line length[18], faster evaporation of the microlayer[17], enhanced capillary wicking[14,21], and coupling/competition between multiple phenomena such as rewetting-heating[20], wicking-evaporation,[22] and wicking-conduction[19]. Of the many theories that have been put forward, the strong role of capillary wicking has been experimentally verified[14] in combination with multiple observations of wicking underneath bubbles during boiling[18,20,23]. While there is now a consensus that capillary wicking is the predominant CHF enhancement mechanism in microstructured surfaces, a clear understanding of reasons underlying heat transfer coefficient enhancement from such surfaces is still lacking. Such an enhancement is often attributed to a nucleation site density increase due to surface roughness[6]. However, studies have shown that different surfaces having similar roughness can have vastly different boiling performance, revealing the need for alternate explanations[5,16,24]. One such alternative explanation when using highly ordered microstructured surfaces is a surface area enhancement (fin effect)[21]. However, these suggested enhancement mechanisms do not account for all salient physical heat transfer mechanisms that contribute to boiling.

The high heat transfer coefficients obtained during pool boiling on a horizontal surface have been attributed to several mechanisms including microlayer evaporation, bulk evaporation,

contact line evaporation, transient conduction, and microconvection[25]. Many studies have leveraged microheater arrays[26], liquid crystals[27], MEMS sensors[28], interferometry[29], IR measurements[30], and numerical simulations[31] to delineate the contribution of each different mechanism to the overall heat transfer, but there remains an open debate about the governing factor[32]. Evaporation from the microlayer[33], a thin layer of liquid trapped underneath a rapidly expanding bubble during boiling is of particular relevance as it is known to be enhanced by capillary wicking in microstructured surfaces[14,18,23]. Recent visualizations using synchrotron X-ray[23] and through-bubble endoscopy[18] have shown the existence of a liquid microlayer underneath the bubbles during boiling on microstructured surfaces. In contrast to a non-uniform microlayer thickness on bare hydrophilic surfaces as first suggested by Cooper and Lloyd[34], microstructured surfaces have liquid trapped between all of the structures by capillary action to form a uniform thickness microlayer throughout the entire area beneath the bubble[23]. We hypothesize that enhanced evaporation from the microlayer due to the presence of microstructures is the predominant mechanism of the heat transfer coefficient enhancement observed from microstructured surfaces during boiling.

In the present work, we show that the contribution of microlayer evaporation to the heat transfer coefficient enhancement can be altered in a controlled manner by tuning the microstructured surface morphology. Highly ordered micropillared wicking surfaces are fabricated on silicon surfaces and pool boiling experiments are performed. The regularity of surfaces allows for analytical prediction of evaporative heat transfer underneath the bubble (Fig. 1(a)). Through these boiling experiments and analytical prediction of evaporation, we show that the amount of microlayer evaporation from a given surface is the key mechanism that determines the extent of

enhancement in the boiling heat transfer coefficient. This conclusion is an essential step toward *a priori* prediction of heat transfer coefficients for rational design of microstructured boiling surfaces.

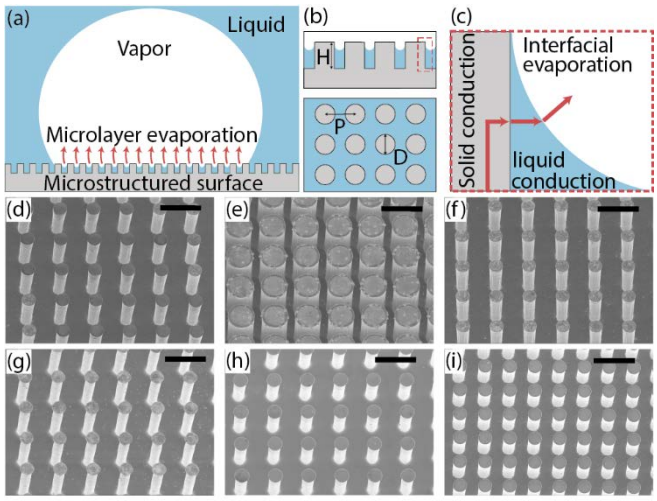

FIG. 1. Illustrations of (a) a single bubble growing during nucleate pool boiling on a microstructured surface, (b) side and top-down views of the specific micropillar array geometry used in the study, and (c) the heat flow path and salient transfer modes during evaporation from a micropillared surface with an imbibed liquid layer (side view). Subfigure parts (d)-(i) show SEM images of the fabricated boiling surfaces numbered S1 to S6, respectively, with dimensional details provided in Table 1. The black scale bar represents 50 μm.

Square arrays of circular micropillars having different pitch, diameter, and height (Fig. 1(b)) are fabricated to explore the influence of these parameters on boiling heat transfer enhancement (fabrication details in Supplemental Material S1). Briefly, 1 cm × 1 cm square surfaces with structures are formed on an undoped silicon wafer using photolithography and deep reactive ion etching (DRIE).. The backside of the samples are coated with thin layers of Cr-Au-Cu, to enable consistent solder-bonding of the substrate to a copper heating block in the boiling test section (experimental details in Supplemental Material S2). The test section is sealed into a boiling

chamber with the substrate submerged in a pool that is maintained at the saturation pressure and temperature. Experiments are performed with degassed HFE-7100 as the working fluid at a pressure of 101.5 kPa, corresponding to a saturation temperature of 60 ˚C. During boiling experiments, the surface is heated at increasing power inputs using cartridge heaters in the test section and the steady-state surface temperatures (T_{surf}), pool temperatures (T_{pool}) , superheats ($\Delta T = T_{surf} - T_{pool}$) and heat fluxes ($q''$) are recorded using embedded thermocouples in the heater block. All thermocouples are calibrated and the uncertainty in calculated surface superheat and heat flux are typically ±0.35 ˚C and ±1.28 W cm^{-2}, respectively (calibration and uncertainty analysis details in Supplemental Material S3). Side view high-speed visualizations at 3000 frames per second are recorded for all the experiments .

Key dimensions of the surfaces are presented in Table 2 are characterized by measuring the diameter and pitch using a microscrope, and the height using an optical profilometer.. Scanning electron microscope images (SEM) are taken after the experiments for inspection and are shown in Fig. 1(d)-(i). The surfaces are designed so that the effect on evaporative performance from variation of a specific parameter (while holding other parameters constant) can be investigated. These include variations in the pillar diameter-to-pitch ratio D/P (S2–S3–S1), height H (S3–S5–S4, and S2–S7–S8), and size where D:P:H is kept constant while scaling the structure (S5–S6). In each category of surfaces in Table 1, the parameter being investigated is emphasized in bold. Two bare surfaces are tested to establish repeatability in the measurements and to serve as an unmicrostructured benchmark (see Supplemental Material S4). Several additional structures are also tested (S9-S11, boiling curves in Supplemental Material S5) to facilitate quantitative assessment of our hypothesis.

The experimentally obtained boiling curves are shown in Fig. 2 for structures S1-S6 grouped by different dimensional effects: (a) diameter-to-pitch ratio (D/P), (b) height (H), and (c) size (at constant P:H:D). The boiling tests for these structured surfaces are conducted over heat fluxes that span the regimes of single-phase natural convection, initiation of nucleate boiling, and nucleate boiling with discrete and coalescing bubbles, all the way to CHF (Supplementary Movies SM1-SM4 illustrate these regimes). The influence of the increasing diameter-to-pitch (D/P) ratio (S2–S3–S1) on the boiling curves is shown in Fig. 2 (a). The boiling curves shift towards the left (lower superheat at a given heat flux) with an increase in D/P reflecting an enhancement in the boiling heat transfer coefficient. Such a shift can be attributed to the enhanced evaporation underneath the bubble. Given a fixed microstructure height (H) and pitch (P), an increase in pillar diameter (and thus D/P ratio) increases the three-phase contact line length per unit area in the microlayer underneath the bubble and decreases the evaporative meniscus area. Over this range of D/P, the net effect is an increasing evaporative performance as quantitatively confirmed in the subsequent discussion.

Table 2. Dimensions of micropillared surfaces tested for pool boiling performance.

Trend	Surface Name	Pitch, P (μm)	Diameter, D (μm)	Height, H (μm)	Diameter / Pitch, D/P
	Bare surface	-	-	-	-
Diameter-to-ptich	S1	40.0	**16.0**	70.2	**0.40**
	S3	40.0	**19.8**	76.9	**0.50**
	S2	40.0	**30.6**	67.3	**0.76**
Height	S3	40.0	19.8	**76.9**	0.50
	S5	40.0	17.5	**89.0**	0.44
	S4	40.0	16.9	**101.0**	0.42
Size	S5	**40.0**	**17.5**	**89.0**	**0.44**
	S6	**30.0**	**16.5**	**67.9**	**0.55**
Height	S2	40.0	30.6	**67.3**	0.76
	S7	40.0	31.0	**85.0**	0.78
	S8	40.0	30.5	**91.0**	0.76
Additional Structures	S9	30.0	11.7	94.0	0.39
	S10	24.0	14.5	91.0	0.60
	S11	12.0	6.1	67.0	0.51

Increasing the height of the microstructures with pitch and diameter kept constant (S3–S5–S4) shifts the boiling curves to the right (Fig. 2 (b)), reflecting a reduction in boiling heat transfer coefficient. This reduction can be attributed to reduced microlayer evaporation, due to an expected increase in the thermal resistance to heat flow with an increase in height of the pillars. An additional set of structures (S2–S7–S8) are also studied and confirm this trend with height (Supplemental Material S5).

The influence of the structure size (S5–S6) is explored in Fig. 2 c. The boiling curves shift rightward with increase in pillar size reflecting a reduced heat transfer coefficient. An increase in pillar size results in reduced evaporative performance as both the three-phase contact line length per unit area and the thermal conductance decrease.

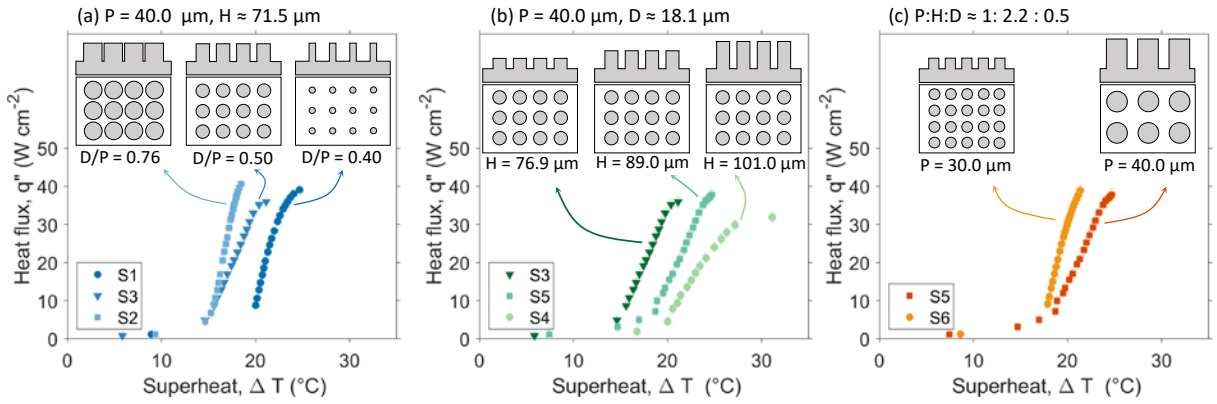

FIG. 2 Boiling curves (heat flux versus superheat) for structures S1 to S6 plotted in three groups of parameter variations: (a) different D/P ratios with P = 40.0 µm and H ≈ 71.5 µm (S2–S3–S1), (b) different heights with P = 40.0 µm and D ≈ 18.1 µm (S3–S5–S4), and (c) different sizes at constant P:H:D ≈ 1:2.2:0.5 (S5–S6). The insets depict the side and top views of the respective surface for each boiling curve and highlight the parameters varied. The error bars depict the uncertainty in the boiling curves.

The parametric trends discussed above point to a dependence of the boiling heat transfer on microlayer evaporation. Alternative potential mechanisms for the enhancement observed could be an increase in nucleation site density and bubble departure frequency due to increase in surface roughness[6], or the fin effect leading to an increase insurface area[21]. Either of these enhancement mechanisms would imply a positive correlation to some roughness parameter. However, the trends observed in the present study show a decrease in heat transfer coefficient with an increase in micropillar size or height (and thereby roughness) in Fig. 2 b and c. The results therefore invalidate these alternative mechanisms because the heat transfer enhancement on structured surfaces is not simply correlated to a traditional measure of roughness.

The thorough exploration of parametric trends in Fig. 2 reveals a consistent behavior of enhanced heat transfer coefficient tied to the efficacy of evaporation underneath the bubbles due

to microstructuring. To further test this deduction, we now analytically model the evaporative performance of the surface and show its influence on the boiling heat transfer coefficient. To construct our model for the evaporative performance of a microstructured surface, we assume that the surface is well-fed with liquid by capillary action such that all the pores on the surface contain liquid menisci. The evaporative heat transfer coefficient, defined as the heat flux dissipated per unit surface superheat, is used as the metric for evaporative performance of the surface. We use an analytical model we previously developed [35], which considers a structured surface wetted with a liquid that maintains a meniscus of constant curvature. The heat conducts through the pillars up to the location of the meniscus, where it conducts across the liquid thin film and is dissipated by evaporation (Fig. 1(c)). Heat flux dissipated from the microstructure is evaluated by integrating the heat dissipated over the entire liquid meniscus area. The thermal resistance to evaporation of the structured surface (R_{lv}), considering the effects of resistance across the thin-liquid film and the liquid-vapor interface, is given by

$$\frac{1}{R_{\mathrm{lv}}} = \int_0^{\left(P^*-D\right)\left(1-\sin\theta\right)/\left(2\cos\theta\right)} \frac{2\pi\left(D/2+\delta\right)\sqrt{1+\delta'^2}\,h_{\mathrm{m}}}{1+\sqrt{1+\delta'^2}\left(D/2+\delta\right)\ln\left(\dfrac{D/2+\delta}{D/2}\right)\dfrac{h_{\mathrm{m}}}{k_{\mathrm{l}}}}\,dy \tag{1}$$

Here, δ is the local thickness of the meniscus, θ is the contact angle, and h_m is the intrinsic evaporative heat transfer coefficient at the interface calculated using Schrage's expression[35,36]. The thermal resistance due to conduction along the height of the pillars is added in series to obtain the final expression for the evaporative heat transfer coefficient (h_{evap})

$$h_{\mathrm{evap}} = \frac{1}{R_{lv}A + \left(H/k_{\mathrm{eff}}\right)} \tag{2}$$

Here, A is the area of the unit cell and $k_{\text{eff}} (= \varepsilon k_l + (1-\varepsilon) k_s)$ is the effective thermal conductivity expressed in terms of porosity ε, and solid (k_s) and liquid (k_l) thermal conductivities.

Equation (2) is then incorporated into an expression for the boiling heat flux to assess the relative contribution of the microlayer evaporative heat transfer with respect to other heat transfer mechansims like microconvection, transient conduction, bulk evaporation, and contact line evaporation. For a microstructured surface, we assume that these other mechanisms provide no relative enhancement compared to a bare surface, and therefore decompose the total heat flux dissipated into the heat flux on the bare surface by all other dissipation mechanisms (q''_{bare}) and the enhancement due to additional microlayer evaporation offered by the microstructures ($q''_{\text{microlayer}}$):

$$q'' = q''_{\text{bare}} + q''_{\text{microlayer}} \tag{3}$$

At a given superheat, the bare surface heat flux is obtained from the bare surface experimental boiling curve (Supplemental Material S4). The enhancement due to microlayer evaporation from the microstructures is expressed in terms of the predicted evaporative heat transfer coefficient (h_{evap}) as

$$q''_{\text{microlayer}} = \frac{A_{\text{microlayer}}}{A_{\text{total}}} h_{\text{evap}} \Delta T \tag{4}$$

where the ratio $A_{\text{microlayer}} / A_{\text{total}}$ is the spatiotemporal average fraction of the heated area that is occupied by the microlayer. Using equations (3) and (4), the microlayer area fraction ($A_{\text{microlayer}} / A_{\text{total}}$) can be written as

$$\frac{A_{\text{microlayer}}}{A_{\text{total}}} = \frac{q''_{\text{surf}} - q''_{\text{bare}}}{h_{\text{evap}}\Delta T} \tag{5}$$

This microlayer area fraction is extracted from the experimentally measured heat fluxes and superheats for all the structured surfaces relative to the baseline bare surface, as shown in Fig. 3(a). This parameter collapses across all surfaces onto a linear relationship (within ± 30% of $A_{\text{microlayer}} / A_{\text{total}} = 0.0043q''$), indicating that the primary mechanism influencing different microstructured surfacers is microlayer evaporation. The area fraction increases with heat flux, with a dip near CHF due to partial dryout of the surface. Some scatter in the calculated microlayer area fraction data is expected due to the complex influences of bubble size, density, and frequency, which can be affected by the microstructure. Any changes in these bubble ebullition characteristics could affect the boiling heat transfer by altering the contact line dynamics and relative contributions of different heat transfer mechanisms such as bulk evaporation, transient conduction, or microconvection[32]. However, the collapse of different boiling curves based on evaporation heat transfer coefficient alone in Fig. 3(a) suggests that the primary enhancement mechanism is indeed a result of increased microlayer evaporation from these microstructured surfaces.

For the purpose of showcasing the effect of enhanced microlayer evaporation on boiling, a basic relation that captures the influence of the microstructure evaporation on the boiling heat transfer can be obtained by substituting the linear fit of microlayer area fraction in equation (4) into equation (3).

$$q'' = \frac{q''_{\text{bare}}}{1 - (0.0043 h_{evap}\Delta T)} \tag{6}$$

The terms on the right side of equation (6) are functions only of fluid properties and surface geometry (h_{evap}), superheat (ΔT), and the bare surface reference boiling curve ($q''_{\text{bare}}(\Delta T)$). Equation (6) is used to plot the boiling curves (dashed lines) for two microstructured surfaces of highest and lowest evaporative heat transfer coefficients along with the experimental data points in Fig. 3(b). As the evaporative heat transfer coefficient of the surface increases, a shift is observed in the experimental boiling curves towards the left reflecting an enhancement in boiling heat transfer coefficient. This enhancement is captured by the relationship between evaporation and boiling heat transfer coefficients in Equation (6) (dotted lines in Fig. 3(b)). The predicted evaporation heat transfer coefficient value is a function of the accommodation coefficient ($\sigma = 1$ is used for HFE -7100, with detailed information on the thermophysical properties provided Supplemental Material S6); however, this accommodation coefficient only rescales the values in Fig. 3(a) without affecting the conclusions. The value of fitting factor in the denominator of the relationship for boiling heat flux developed in Equation (6) would rescale appropriately such that the boiling heat flux predictions in Fig. 3(b) are invariant of accommodation coefficient.

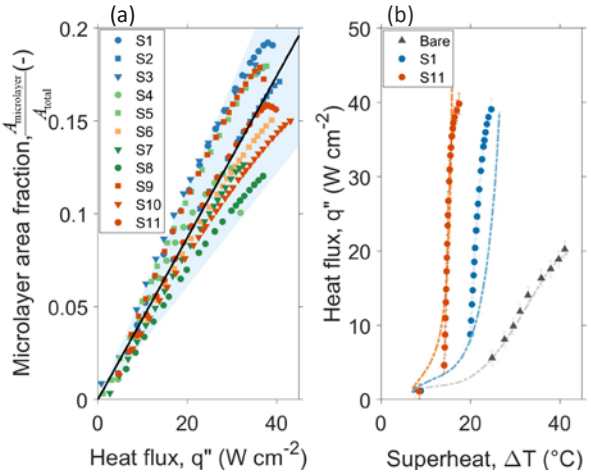

FIG. 3 (a) Microlayer area fraction plotted as a function of heat flux for all the structured surfaces studied. (b) Boiling curves for the bare silicon surface and microstructured surfaces S1 and S11

with the lowest and highest respective evaporative heat transfer coefficients. The dotted-line predictions for the microstructured surfaces are from Eq.(6).

Heat transfer coefficients during boiling ($h_{boil} = q'' / \Delta T$), defined as the heat flux per unit superheat for different structured surfaces are calculated directly from the experimental measurements at three different heat fluxes (10, 20, and 30 W cm^{-2}) and plotted against the evaporative heat transfer coefficient (h_{evap} , Eq. (2)) in Fig 4. The error bars represent the maximum uncertainty in the heat transfer coefficients (Supplemental Material S3). To further assess whether these conclusions regarding the microlayer enhancement extend more generally to other working fluids, the experimental boiling heat transfer coefficients from Kim et al.[21] for boiling of water on microstructured silicon at 50 W cm^{-2} are also plotted in Fig 4. Across all datasets, a positive correlation between the evaporation heat transfer coefficient and the boiling heat transfer coefficient is observed; the Pearson's correlation coefficient, a measure of the linearity between these two parameters, is + 0.728, + 0.794, + 0.814, and + 0.877 at 10, 20, 30, and 50 W cm^{-2}, respectively. At a given heat flux, higher h_{evap} yields an increase in h_{boil} as the enhanced microlayer evaporation underneath bubbles due to the presence of the microstructures results in a commensurate reduction in surface temperature needed to dissipate a given heat flux. This confirms that the microlayer evaporation underneath the bubble is the predominant mechanism of enhancement.

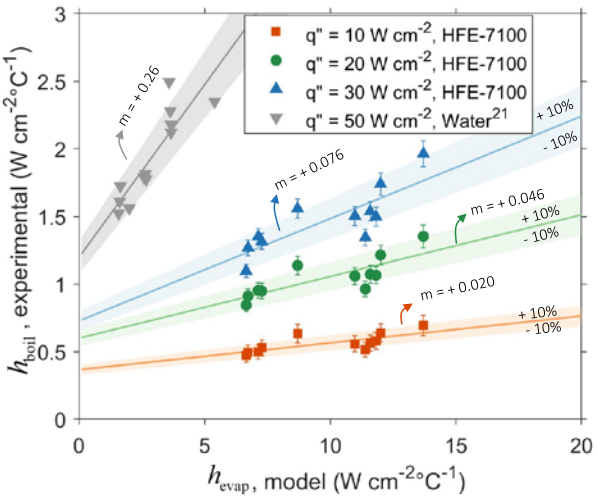

FIG. 4 Boiling heat transfer coefficients (h_{boil}) for the microstructured surfaces from experiments with HFE-7100 at three different heat fluxes 10 (red), 20 (green) and 30 (blue) W cm^{-2}, and experimental data[21] from the literature for water at 50 W cm^{-2} (gray) are plotted against the evaporation heat transfer coefficient from Eq. (2) (h_{evap}). Boiling and evaporation heat transfer coefficients are positively related with respective linear fitted slopes of 0.020, 0.046, 0.076 and 0.26 for 10, 20, 30, and 50 W cm^{-2}, respectively. The maximum uncertainty in experimental boiling heat transfer coefficient for the HFE-7100 data is ± 0.095 W cm^{-2} °C^{-1}.

In summary, this work quantifies the contribution of microlayer evaporation from microstructures on a surface to the boiling heat transfer coefficient enhancement achieved. While microlayer evaporation is known to be one of the important mechanisms for single-bubble heat transfer, its overall contribution in boiling is still poorly understood. Boiling curves obtained from custom-fabricated microstructured surfaces in this work are used to deduce a microlayer area fraction, the heat transfer coefficient enhancement normalized with evaporative efficacy of the microstructures, is independent of surface microstructure . A linear relationship between the boiling heat transfer coefficient and the microlayer evaporation is obtained, indicating the

microlayer evaporation as the primary boiling enhancement mechanism. While this work uses a simple empirical relationship to highlight this role, future developments could focus on more comprehensive modeling of evaporation from the microlayer and its effect on boiling heat transfer coefficient.

Supplemental Material

See Supplemental Material for surface fabrication, boiling experimental setup and test procedure, thermocouple calibration and uncertainty analysis, bare surface boiling curve and polynomial fit, boiling curves for additional microstructured surfaces, thermophysical properties and high-speed videos of boiling behavior.

Acknowledgement

This work was supported in part by Purdue's NEPTUNE Center for Power and Energy, funded by the Office of Naval Research under Grant No. N000141613109. We thank Rishav Roy for assisting in fabrication of the microstructured surfaces used in the study, and Taylor Allred, Carolina Mira-Hernandez, and Srivathsan Sudhakar for their discussions in building the pool boiling facility.

References

[1] S. Nukiyama, J. Soc. Mech. Eng. Jpn. **37**, 367 (1934).
[2] B.B. Kanbur, C. Wu, S. Fan, W. Tong, and F. Duan, Int. J. Refrig. **118**, 290 (2020).
[3] G. Liang and I. Mudawar, Int. J. Heat Mass Transf. **128**, 892 (2019).
[4] G. Ribatski and J.R. Thome, Appl. Therm. Eng. **26**, 1018 (2006).
[5] B.J. Jones, J.P. McHale, and S.V. Garimella, J. Heat Transf. **131**, 121009 (2009).
[6] J.P. McHale and S.V. Garimella, Exp. Therm. Fluid Sci. **44**, 456 (2013).
[7] J.P. McHale and S.V. Garimella, Exp. Therm. Fluid Sci. **44**, 439 (2013).
[8] J. Kim, S. Jun, R. Laksnarain, and S.M. You, Int. J. Heat Mass Transf. **101**, 992 (2016).
[9] T.P. Allred, J.A. Weibel, and S.V. Garimella, Phys. Rev. Lett. **120**, 174501 (2018).
[10] H. Kim and D.E. Kim, Int. J. Heat Mass Transf. **180**, 121762 (2021).
[11] S.G. Liter and M. Kaviany, Int. J. Heat Mass Transf. **44**, 4287 (2001).

[12] S. Sarangi, J.A. Weibel, and S.V. Garimella, J. Heat Transf. **139**, (2016).
[13] R. Chen, M.-C. Lu, V. Srinivasan, Z. Wang, H.H. Cho, and A. Majumdar, Nano Lett. **9**, 548 (2009).
[14] M.M. Rahman, E. Ölçeroğlu, and M. McCarthy, Langmuir **30**, 11225 (2014).
[15] K.-H. Chu, R. Enright, and E.N. Wang, Appl. Phys. Lett. **100**, 241603 (2012).
[16] R.I. Vachon, G.E. Tanger, D.L. Davis, and G.H. Nix, J. Heat Transf. **90**, 231 (1968).
[17] A. Zou, D.P. Singh, and S.C. Maroo, Langmuir **32**, 10808 (2016).
[18] J. Li, G. Zhu, D. Kang, W. Fu, Y. Zhao, and N. Miljkovic, Adv. Funct. Mater. **31**, 2006249 (2021).
[19] M. Tetreault-Friend, R. Azizian, M. Bucci, T. McKrell, J. Buongiorno, M. Rubner, and R. Cohen, Appl. Phys. Lett. **108**, 243102 (2016).
[20] N.S. Dhillon, J. Buongiorno, and K.K. Varanasi, Nat. Commun. **6**, 8247 (2015).
[21] S.H. Kim, G.C. Lee, J.Y. Kang, K. Moriyama, M.H. Kim, and H.S. Park, Int. J. Heat Mass Transf. **91**, 1140 (2015).
[22] H. Hu, J.A. Weibel, and S.V. Garimella, Int. J. Heat Mass Transf. **136**, 373 (2019).
[23] D.I. Yu, H.J. Kwak, H. Noh, H.S. Park, K. Fezzaa, and M.H. Kim, Sci. Adv. **4**, e1701571 (2018).
[24] K. Ferjančič and I. Golobič, Exp. Therm. Fluid Sci. **25**, 565 (2002).
[25] J. Kim, Int. J. Multiph. Flow **35**, 1067 (2009).
[26] J.G. Myers, V.K. Yerramilli, S.W. Hussey, G.F. Yee, and J. Kim, Int. J. Heat Mass Transf. **48**, 2429 (2005).
[27] C. Sodtke, J. Kern, N. Schweizer, and P. Stephan, Int. J. Heat Mass Transf. **49**, 1100 (2006).
[28] S. Moghaddam, K.T. Kiger, A. Modafe, and R. Ghodssi, J. Microelectromechanical Syst. **16**, 1355 (2007).
[29] Z. Chen, X. Hu, K. Hu, Y. Utaka, and S. Mori, Int. J. Heat Mass Transf. **146**, 118856 (2020).
[30] S. Jung and H. Kim, Int. J. Heat Mass Transf. **120**, 1229 (2018).
[31] Z. Chen, F. Wu, and Y. Utaka, Int. J. Heat Mass Transf. **118**, 989 (2018).
[32] P.A. Raghupathi and S.G. Kandlikar, Int. J. Heat Mass Transf. **95**, 296 (2016).
[33] F.D. Moore and R.B. Mesler, AIChE J. **7**, 620 (1961).
[34] M.G. Cooper and A.J.P. Lloyd, Int. J. Heat Mass Transf. **12**, 895 (1969).
[35] M. Bongarala, H. Hu, J.A. Weibel, and S.V. Garimella, Int. J. Heat Mass Transf. **182**, 121964 (2022).
[36] R.W. Schrage, *A Theoretical Study of Interphase Mass Transfer* (Columbia University Press, 1953).